An X-ray counterpart of HESS J1427–608 discovered with Suzaku

Takahisa Fujinaga,[1,2] Koji Mori,[3] Aya Bamba,[4] Shoichi Kimura,[3] Tadayasu Dotani,[2,1,5]
Masanobu Ozaki,[2] Keiko Matsuta,[5,2] Gerd Pühlhofer,[6] Hideki Uchiyama,[7] Junko S. Hiraga,[7]
Hironori Matsumoto,[8] and Yukikatsu Terada[9]

[1]*Department of Physics, Tokyo Institute of Technology, 2-12-1 Ookayama, Meguro-ku, Tokyo 152-8550*

[2]*Institute of Space and Astronautical Science, Japan Aerospace Exploration Agency,*

3-1-1 Yoshinodai, Chuo-ku, Sagamihara, Kanagawa 252-5210

fujinaga@astro.isas.jaxa.jp

[3]*Department of Applied Physics and Electronic Engineering, University of Miyazaki, 1-1 Gakuen
Kibanadai-Nishi, Miyazaki, 889-2192*

[4]*Department of Physics and Mathematics, Aoyama Gakuin University, 5-10-1 Fuchinobe, Chuo-ku,
Sagamihara, Kanagawa 252-5258*

[5]*Department of Space and Astronautical Science, The Graduate University for Advanced Studies,
3-1-1 Yoshinodai, Chuo-ku, Sagamihara, Kanagawa 252-5210*

[6]*Institut für Astronomie und Astrophysik, Universität Tübingen, Sand 1, D 72076 Tübingen, Germany*

[7]*The University of Tokyo, 7-3-1 Hongo, Bunkyo-ku, Tokyo 113-0033*

[8]*Nagoya University, Furo-cho, Chikusa-ku, Nagoya 464-8602*

[9]*Saitama University, Shimo-Okubo 255, Sakura-ku, Saitama 338-8570*

Abstract

We report the discovery of an X-ray counterpart of the unidentified very high energy gamma-ray source HESS J1427–608. In the sky field coincident with HESS J1427–608, an extended source was found in the 2–8 keV band, and was designated as Suzaku J1427–6051. Its X-ray radial profile has an extension of $\sigma = 0\rlap{.}'9 \pm 0\rlap{.}'1$ if approximated by a Gaussian. The spectrum was well fitted by an absorbed power-law with $N_{\mathrm{H}} = (1.1 \pm 0.3) \times 10^{23}$ cm^{-2}, $\Gamma = 3.1^{+0.6}_{-0.5}$, and the unabsorbed flux $F_{\mathrm{X}} = (9^{+4}_{-2}) \times 10^{-13}$ erg s^{-1} cm^{-2} in the 2–10 keV band. Using XMM-Newton archive data, we found seven point sources in the Suzaku source region. However, because their total flux and absorbing column densities are more than an order of magnitude lower than those of Suzaku J1427–6051, we consider that they are unrelated to the Suzaku source. Thus, Suzaku J1427–6051 is considered to be a truly diffuse source and an X-ray counterpart of HESS J1427–608. The possible nature of HESS J1427–608 is discussed based on the observational properties.

1. Introduction

The origin of cosmic rays is an unsolved problem since the discovery in 1912. The spectrum of cosmic rays has a break at the knee energy ($10^{15.5}$ eV), and those below the knee energy are believed to have Galactic origin. Recently, the High Energy Stereoscopic System (H.E.S.S.) found more than 50 sources on the Galactic plane in the very high energy (VHE; $\gtrsim 100$ GeV) gamma-ray band (Aharonian et al. 2005; Aharonian et al. 2006). Because VHE gamma-rays are produced either through inverse Compton scattering of low energy photons by relativistic electrons, or through the decay of pions produced by collisions of relativistic protons with interstellar medium, high energy particles are surely present in the VHE gamma-ray sources. If relativistic electrons are present, they may be traced through the observations of synchrotron X-ray emission. However, in spite of extensive X-ray followup observations, a non-negligible fraction of the Galactic VHE gamma-ray sources do not have an X-ray counterpart, and they are referred to as unidentified (unID) sources (e.g., Fujinaga et al. 2011).

Among identified Galactic VHE gamma-ray sources, pulsar wind nebulae (PWNe) represent the largest population (Hinton & Hoffman 2009). Accordingly, one would expect that PWNe are the first candidate of the origin of the unID VHE gamma-ray sources. However, identifying the VHE gamma-ray sources as PWNe is not straightforward. The VHE gamma-ray emission region sometimes shows significant spatial offset from the X-ray emission region or a pulsar (e.g., de Jager & Djannati-Ataï 2009; Mattana et al. 2009). Furthermore, the life time of X-ray emitting electrons through synchrotron emission may be shorter than that of VHE gamma-ray emitting electrons through Compton scattering. This means that X-ray emission from the PWNe can be much dimmer than the VHE gamma-rays if the PWNe are old. Finally, a pulsar is not always found in the vicinity of (candidate) PWNe.

HESS J1427–608 is one of the unID VHE gamma-ray sources located at $l = 314°.409, b = -0°.145$ (Aharonian et al. 2008), and is extended with $\sigma = 0°.06$[1]. The flux is $F_{\mathrm{TeV}} = 4.0 \times 10^{-12}$ erg s^{-1} cm^{-2} in the 1–10 TeV band with a photon index of $\Gamma = 2.16$ (Aharonian et al. 2008). No plausible counterpart is listed in the Galactic supernova remnant (SNR) catalog (Green 2009) or in the SIMBAD data base[2] in the vicinity of HESS J1427–608. We also looked for a possible counterpart in the ATNF pulsar catalog (Manchester et al. 2005). However, no energetic pulsar was found within $100'$ from HESS J1427–608. Here, the definition of the energetic pulsar is those with $\dot{E}/d^2 > 10^{33}$ erg s^{-1} kpc^{-2}, where $\dot{E}$ is the spin-down energy and d is the distance to the source. This

---

[1] Poster presentation by Komin, N., et al. in "The X-ray Universe 2011" held in June 27–30, 2011, at Berlin, Germany, http://xmm.esac.esa.int/external/xmm_science/workshops/2011symposium/posters/Komin_TopicE.pdf

[2] http://simbad.u-strasbg.fr/simbad/

search radius of $100'$ is large enough compared to offsets of radio pulsars to VHE sources among known PWN systems, and virtually excludes the possibility of associating HESS J1427–608 with any known energetic radio pulsar. Thus, HESS J1427–608 seems to be one of the most "unlikely" PWNe among the VHE gamma-ray sources. In order to search for an X-ray counterpart, we observed HESS J1427–608 with Suzaku, and also analyzed the XMM-Newton archive data.

2. Observation and Data Reduction

We observed the sky region including HESS J1427–608 with Suzaku (Mitsuda et al. 2007) from 2010 January 13 through 16. The journal of the observation is listed in table 1. Suzaku is equipped with two types of detectors: four sets of X-ray Imaging Spectrometers (XIS0–XIS3: Koyama et al. 2007) and a non-imaging Hard X-ray Detector (HXD: Takahashi et al. 2007; Kokubun et al. 2007). XIS1 uses the back-illuminated (BI) CCD while the others the front-illuminated (FI) CCDs. Among the four sensors, XIS2 is not operational[3] and a part of XIS0 (corresponding to the off-source region in the latter analysis) is not usable due to its anomaly[4]. Hereafter, unless otherwise mentioned, we used only XIS1 and XIS3 data for the current analysis. XIS was operated in normal clocking mode without any window options. Spaced-row charge injection (Prigozhin et al. 2008; Uchiyama et al. 2009a) was used to reduce the effects of radiation damage.

We used version 2.4.12.27 of the processed data for HESS J1427–608. The data was analyzed with the HEADAS software version 6.10 and XSPEC version 12.6.0. We used the cleaned event file created by the Suzaku team. The resultant effective exposure was 104 ks.

3. Analysis

3.1. Images

Figure 1 shows XIS images in the soft (0.5–2 keV) and the hard (2–8 keV) bands. The images were corrected for exposure using an exposure map generated by the FTOOL `xisexpmapgen` after subtracting non X-ray background (NXB) images generated by the FTOOL `xisnxbgen` (Tawa et al. 2008). Finally, the XIS1 and XIS3 images were added, and the resulting image was binned to a pixel size of $8''$ and smoothed with a Gaussian of $\sigma = 1.'0$. The position center and the extent of HESS J1427–608 are shown as a black cross and a yellow dashed circle, respectively. A few faint, point-like sources are seen in the soft band, while an apparently extended source is detected in the hard band. The position and apparent extension of the hard source match those of HESS J1427–608. As will be shown in a later section, all the Suzaku soft-band sources may be explained by the point-like sources in the XMM-Newton archive data while the Suzaku hard-band source seems to be a truly

---

[3]   JX-ISAS-SUZAKU-MEMO-2007-08;   http://www.astro.isas.jaxa.jp/suzaku/doc/suzakumemo/suzakumemo-2007-08.pdf

[4]   JX-ISAS-SUZAKU-MEMO-2010-01;   http://www.astro.isas.jaxa.jp/suzaku/doc/suzakumemo/suzakumemo-2010-01.pdf

new source. We thus designate the central hard-band source Suzaku J1427–6051, and mainly focus on this source in the following analysis.

Because HESS J1427–608 and Suzaku J1427–6051 are both extended, we evaluate the X-ray size of the source. For this purpose, careful estimation of the X-ray background is necessary since Suzaku J1427–6051 is relatively faint. In particular, this region contains significant contribution from the Galactic ridge X-ray emission (GRXE) as well as the cosmic X-ray background (CXB), both of which are subject to mirror vignetting effect resulting in a centrally-peaked spatial distribution. Therefore, it is not appropriate to assume a flat background image defined at an off-source region within the field of view (FOV). Instead, we estimated the GRXE+CXB image in the source region through Monte-Carlo simulation. We explain details of the X-ray background estimation below.

First, we estimated the surface brightness of the GRXE and CXB assuming their uniform distribution in the sky. For this purpose, we analyzed the X-ray spectrum in the off-source annulus region shown in figure 2. The region (between $6'.5$ and $7'.5$ from the center of Suzaku J1427–6051) was selected to minimize contamination from Suzaku J1427–6051. In other words, the off-source region contains only the GRXE and the CXB after the subtraction of NXB. Figure 3 shows the spectra extracted from the off-source region. The spectra were modeled by optically thin thermal three temperature plasma with neutral iron emission line plus the CXB following Uchiyama et al. (2009b). In the course of model fitting, the hydrogen column density was fixed to $1.54 \times 10^{22}\,\mathrm{cm}^{-2}$ determined by H I observations (Kalberla et al. 2005), the photon index of the CXB to 1.4, and the surface brightness of the CXB to $5.4 \times 10^{-15}\,\mathrm{erg\,s}^{-1}\,\mathrm{cm}^{-2}\,\mathrm{arcmin}^{-2}$ in the 2–10 keV band (Kushino et al. 2002). We made the ancillary response file using the FTOOL `xissimarfgen` assuming a uniform emission in the sky. The model could reproduce the observed spectrum well. The best-fit parameters are listed in table 2.

Next, we simulated the GRXE+CXB event data assuming uniform emission with the best-fit spectrum model determined above using the FTOOL `xissim` (Ishisaki et al. 2007). In order to avoid an extra ambiguity due to poor statistics, the exposure time for the simulation was set to 500 ks. Then we extracted the GRXE+CXB spectrum in the source region and added it to the NXB in the source region to obtain the total background spectrum, following the instruction in section 5.5.2 of the Suzaku technical description[5]. Figure 4 shows the simulated background spectra of the XIS1 and XIS3 respectively as well as the source and off-source spectra. As can be seen from the spectra, the source region contains significant emission above the GRXE+CXB level.

Figure 5 shows the radial profiles of the NXB-subtracted image and the simulated GRXE+CXB image in the 2–8 keV band. The difference is attributed to Suzaku J1427–6051. Even if we consider the relatively broad half-power radius ($1'.0$; Serlemitsos et al. 2007) of the point spread function of Suzaku mirror, Suzaku J1427–6051 is clearly extended. In order to estimate the source extent, we compared the observed radial profile with that of a model calculation for an extended source having a 2D-gaussian distribution. Instead of performing the χ^2 fitting, we calculated χ^2 for a set of

---

[5] http://heasarc.gsfc.nasa.gov/docs/suzaku/prop_tools/suzaku_td/node8.html#SECTION0085200000000000

σ, i.e. $0\rlap{.}'5$, $0\rlap{.}'7$, $0\rlap{.}'8$, $0\rlap{.}'9$, and $1\rlap{.}'1$. The simulated profiles were generated with `xissim`. It turned out that none of them gave an acceptable fit; the radial profile of Suzaku J1427–6051 has a core and a tail in comparison with the best-fit simulation data. We thus performed the χ^2 test using only the core region ($r < 2\rlap{.}'0$). We then could obtain an acceptable fit ($\chi^2 = 0.6$ for 3 degrees of freedom). The best-fit value obtained was $\sigma = 0\rlap{.}'9 \pm 0\rlap{.}'1$ with 90% confidence level.

3.2. Pulsations

Although Suzaku J1427–6051 is extended, we tried to search for pulsations in the XIS light curve as point sources may be hidden in the image. We extracted light curves of the source region in the 0.5–10 keV band and binned them to a time resolution of 16 sec. We calculated Fourier power spectra every 2048 bin ($\simeq 9.1$ hour) using the FTOOL `powspec` to obtain the ensemble-averaged power spectrum density (PSD). The PSD of XIS1 is dominated by the orbital period of the satellite and its higher harmonics, probably due to the contamination of earth albedo. Thus we used only the PSD of XIS3 in the subsequent analysis. No significant peak was detected in the PSD with an upper limit of ~ 10 (Poisson fluctuation level was normalized to 2.0), which corresponds to an rms amplitude of 0.0064 count s^{-1}. Because the net count rate of the source is 0.021 count s^{-1}, this corresponds to a relative amplitude of 31%. Thus we conclude that no coherent pulsation is present in the light curves of Suzaku J1427–6051 with an upper limit of 31 % between the pulse periods of 32 sec and 32768 sec.

3.3. Energy spectra

Figure 6 shows the background-subtracted energy spectra of Suzaku J1427–6051. Here, the background spectrum (sum of GRXE, CXB, and NXB) was calculated with the method detailed in section 3.1. It is found that the spectrum of Suzaku J1427–6051 is featureless and heavily absorbed. Although a hint of feature is seen in the 6–7 keV band, which may be due to the spacial variation of the iron emission line in GRXE, it is not statistically significant. We calculated the ancillary response file using the FTOOL `xissimarfgen` for an extended source of a Gaussian profile with $\sigma = 0\rlap{.}'9$. The spectrum was well modeled by either an absorbed power-law or a thermal model, whose best-fit parameters are listed in table 3. However, a thermal origin is unlikely because the abundance is unreasonably small, and the X-rays are thus considered to be produced by non-thermal processes. The absorbed X-ray flux of the source is 3.1×10^{-13} erg s^{-1} cm^{-2} in the 2–10 keV band.

We also analyzed the spectrum of the HXD to search for emission of Suzaku J1427–6051 above 10 keV. We used the background spectrum called "bgd_d" provided by the Suzaku team (Fukazawa et al. 2009) and added the CXB to it using the FTOOL `hxdpinnxbpi`. We used the XIS nominal-position response file categorized to epoch 6, released as a CALDB. We made the background-subtracted spectrum and fitted it with a power-law, whose photon index was fixed to $\Gamma = 3.1$, as derived from the XIS analysis. The flux in the 15–40 keV band is $(1.6 \pm 1.1) \times 10^{-12}$ erg s^{-1} cm^{-2} (χ^2/d.o.f. = 35.21/27) if no systematic error is taken into account. Based on Fukazawa et al. (2009), who showed the reproducibility of NXB in the 15–40 keV band is about

5

3% in the 90% confidence range, we constructed the NXB spectra with 3% higher count rates to include the systematic error of the NXB reproduction. Then, a significant signal is no longer detected. We thus obtained the 90% upper limit of 5.3×10^{-12} erg s^{-1} cm^{-2} in the 15–40 keV band.

4. Archival data of XMM-Newton

In order to estimate the contribution of point sources, we analyzed the archival data of XMM-Newton including the HESS J1427–608 field. XMM-Newton (Jansen et al. 2001) carries three X-ray telescopes each equipped with a European Photon Imaging Camera (EPIC) at the foci. EPIC consists of two MOS CCD camera (MOS1 and MOS2: Turner et al. 2001) and a pn CCD camera (pn: Strüder et al. 2001). The observation was carried out on 2007 August 9 for 24 ks. During the observation, EPIC was operated in full-frame mode with medium filter.

The data were analyzed with the Science Analysis Software (SAS) version 10.0.0, HEADAS version 6.10 and XSPEC version 12.6.0. Time intervals of enhanced background, which are caused by soft proton flares, were removed with thresholds of 0.20 count s^{-1} for MOS1, 0.24 count s^{-1} for MOS2, and 0.6 count s^{-1} for pn, respectively, calculated for PATTERN=0 events above 10 keV. We used X-ray events of PATTERN=0–12 (for MOS cameras) and PATTERN=0–4 (for pn camera) for the image and spectral analyses. The resultant effective exposures were 21 ks (MOS1), 22 ks (MOS2), and 15 ks (pn), respectively. The journal of the observation is listed in table 1.

4.1. Images

Figure 7 shows the summed images of MOS1 and MOS2 in the soft (0.3–2 keV) and the hard (2–12 keV) bands. The XIS images are also overlaid in green contours. Using the SAS tool `edetect_chain`, a total of 16 point sources were detected within $9'$ from the center of Suzaku J1427–6051. Eleven and seven sources were found in the soft and the hard bands, respectively, and two sources were commonly detected in both bands. Names and count rates of the point sources are listed in table 4. Summing up the count rates of the point sources located within the Suzaku source region (X1 through X7), we obtained $(3.4 \pm 0.4) \times 10^{-3}$ count s^{-1} in the 0.5–2 keV band. This may be converted to the XIS BI count rate of $(2.4 \pm 0.3) \times 10^{-3}$ count s^{-1} assuming the power-law spectrum in table 2. Because this is comparable to the rate actually observed with Suzaku $((3.0 \pm 0.2) \times 10^{-3}$ count s$^{-1})$, the XIS data may be explained by the sum of the XMM-Newton point sources in the soft band. On the other hand, if we carry out a similar calculation for the hard band, the XMM-Newton point sources would produce 7×10^{-4} count s^{-1} in XIS. Because this corresponds to only $\simeq 8$ % of the actual XIS count rate, Suzaku J1427–6051 is difficult to be explained by the sum of the sources and may be a truly diffuse source.

4.2. Energy Spectra

We calculated the energy spectra of only X1 and of the summed spectra of the central seven point sources (X1 through X7). We made the response file and the ancillary response file using the

SAS tool `rmfgen` and `arfgen`, respectively. We fitted these spectra with the model of an absorbed power-law. Because of the poor statistics, the photon index was fixed to 3.1, which was determined by the spectral analysis of Suzaku J1427–6051. The best-fit parameters are listed in table 5. Figure 8 shows the summed spectra of the seven point sources. The absorbed X-ray flux of the summed spectra was 1.7×10^{-14} erg s^{-1} cm^{-2} in the 2–10 keV band, which is about 5% of the flux derived with Suzaku for Suzaku J1427–6051. It is also found that the column density of the summed spectra is two orders of magnitude smaller than that derived for Suzaku J1427–6051. These results confirm that Suzaku J1427–6051 cannot be explained by the XMM-Newton point sources.

5. Discussion

5.1. X-ray and Multi-Wavelength View of HESS J1427–608

We discovered an apparently-diffuse hard X-ray source, Suzaku J1427–6051 with Suzaku, and several point sources with XMM-Newton in spatial coincidence with HESS J1427–608. We found that Suzaku J1427–6051 could not be explained by the sum of the point sources detected with XMM-Newton, and concluded that it is a truly diffuse source. Even if time variability of the detected point-like sources is considered, it is unlikely that Suzaku J1427–6051 is explained by them because the hydrogen column densities are quite different. The XMM-Newton point sources are most likely foreground sources. To explain Suzaku J1427–6051 by the sum of several point sources would require that all those sources would be below detection threshold at the time of the XMM-Newton observation, which appears very unlikely. Thus, we concluded that Suzaku J1427–6051 is an intrinsically diffuse source and the X-ray counterpart of HESS J1427–608.

We searched various catalogs and literature for the possible counterpart of HESS J1427–608 in other wavebands. A GeV gamma-ray source, 2FGL J1427.6–6048c, is listed in the 2-year catalog of Fermi (Nolan et al. 2012). The GeV source is located at $l = 314°3953, b = -0°0909$, which is $3'.3$ away from the center of HESS J1427–608 (see figure 1). Since the error radius of the position is about $3'.6$, it may be associated with HESS J1427–608 (Nolan et al. 2012). However, this is a "c-designator-applied" Fermi source whose position, emission characteristics, or even existence may not be reliable due to a potential confusion with interstellar emission (Nolan et al. 2012). We believe it is premature to discuss a possible association of the GeV source to HESS J1427–608; future Fermi data and analysis is necessary. We also searched the AKARI Point Source Catalogues (Ishihara et al. 2010; Yamauchi et al. 2011). No point source was found in the mid-infrared (9 μm) and the far-infrared (90 μm) bands within $1'.5$ from the center of HESS J1427–608.

5.2. Possible Nature of HESS J1427–608

Although we mentioned HESS J1427–608 as one of the most "unlikely" PWNe in the introduction, its center-filled morphology and featureless spectrum in the X-ray band suggest that the source could be a PWN. Thus we postulate here that the source is a PWN as a working hypothesis. Figure 9 shows the spectral energy distribution (SED) from X-rays to VHE gamma-rays. The esti-

7

mated synchrotron spectra from the VHE gamma-ray spectrum (Aharonian et al. 2008), assuming that the same electron population would inverse-Compton scatter CMB photons up to VHE gamma-rays and radiate synchrotron emission in X-rays, are also plotted with a local magnetic field B of 1, 3, and 10 μG. This SED plot indicates that the simple one-zone leptonic model with B of about 5 μG would roughly explain both the X-ray and VHE gamma-ray data. In this context, the steep Suzaku spectrum of $\Gamma \simeq 3.1$ could indicate that the Suzaku energy band is higher than the cut-off energy. The inferred magnetic field strength of $\simeq$5 μG is within the range of typical values on the Galactic plane. Thus the SED is consistent with a one-zone leptonic model expected for PWNe. We next examine the flux ratio and luminosities. The X-ray to VHE gamma-ray ratio is useful to probe the nature of unID sources (Yamazaki et al. 2006). In the case of HESS J1427–608, the unabsorbed X-ray flux F_X of 8.9×10^{-13} erg s^{-1} cm^{-2} (2–10 keV) and the VHE gamma-ray flux F_{TeV} of 4.0×10^{-12} erg s^{-1} cm^{-2} (1–10 TeV) result in a flux ratio of $F_{\mathrm{TeV}}/F_X \simeq 4.5$. If we assume a distance to HESS J1427–608 of $d = 8$ kpc, the X-ray luminosity would be $L_X = 7 \times 10^{33}$ erg s^{-1}. The estimated flux ratio and X-ray luminosity are within the values of known X-ray and VHE gamma-ray emitting PWNe, given that both values show a large scatter: $10^{-3} - 10^2$ in F_{TeV}/F_X and $10^{32} - 10^{37}$ erg s^{-1} in L_X (Mattana et al. 2009). Thus the flux ratio and luminosity are also consistent with sources of PWN origin.

While there are observational evidences supporting the PWN origin as discussed above, others challenge such a view. With the assumption of $d = 8$ kpc, the core size and whole radial extent would be 2 pc and 12 pc, respectively. The core size of 2 pc is a little large, but not exceptional among other PWN (Kargaltsev & Pavlov 2008). The whole extent of 12 pc is not surprisingly large compared with the nebula of e.g., PSR J1826–1334 (Uchiyama et al. 2009b). The largest drawback of the PWN hypothesis is lacking the detection of both a pulsar and radio PWN associated. It is known that the pulsar luminosity and its nebula luminosity in the X-ray band are correlated over 7 orders of magnitude (Kargaltsev & Pavlov 2008). According to the correlation, the not-yet-detected pulsar should be brighter than $\sim 10^{-13}$ erg s^{-1} cm^{-2} in X-rays, one-tenth of the PWN luminosity. Such a pulsar would have been easily detected with XMM-Newton. In addition, the X-ray photon index of the nebula ($\Gamma = 3.1$) is very steep among the known X-ray nebulae most of which have a Γ between 1.2–2.2 (Kargaltsev & Pavlov 2008).

In terms of photon index comparison, non-thermal SNRs might present a more plausible scenario than PWNe. Most of non-thermal SNRs radiate synchrotron X-rays with a photon index of $\Gamma = 2.4 - 3.1$ (Nakamura et al. 2009). The X-ray luminosity and extent are also compatible to synchrotron SNRs (Nakamura et al. 2012). However, the facts that the source has a center-filled morphology in the X-ray band and no detection of the shell structure in the radio band hamper the interpretation as a non-thermal SNR.

In summary, we have not reached a firm conclusion on the nature of HESS J1427–608. PWN and/or non-thermal SNR, which are not necessary exclusive to each other, are the prime candidates but a decisive observational evidence is lacking. Increasing statistics in Fermi data may reveal a pulsation from 2FGL J1427.6–6048c. A deep radio observation would also be helpful if it could

detect pulsations or reveal the morphology of the source.

6. Conclusion

We observed HESS J1427–608 with Suzaku, which is combined with the archival data analysis of XMM-Newton, and obtained following results.

- We discovered an X-ray counterpart, Suzaku J1427–6051, of HESS J1427–608. It is intrinsically extended ($\sigma = 0\farcs9 \pm 0\farcs1$) and has a spectral shape of an absorbed power-law with a photon index of $\Gamma = 3.1^{+0.6}_{-0.5}$.
- Several faint point sources were found in spatial coincidence with HESS J1427–608 using XMM-Newton archival data in the soft X-ray band.
- Observational properties of Suzaku J1427–6051 and HESS J1427–608 are compared with those of known PWNe and non-thermal SNRs. Some properties favor the PWN and/or SNR origin, but the available data are insufficient to draw firm conclusions.

References

Aharonian, F., et al. 2005, Science, 307, 1938

Aharonian, F., et al. 2006, ApJ, 636, 777

Aharonian, F., et al. 2008, A&A, 477, 353

de Jager, O. C., & Djannati-Ataï, A. 2009, in Neutron Stars and Pulsars, ed. W. Becker (Berlin: Springer), 451

Fukazawa, Y., et al. 2009, PASJ, 61, S17

Fujinaga, T., et al. 2011, PASJ, 63, S863

Green, D. A. 2009, Bull. Astr. Soc. India, 37, 45

Hinton, J. A. & Hoffman, W. 2009, ARAA, 47, 523

Ishihara, D., et al. 2010, A&A, 514, A1

Ishisaki, Y., et al. 2007, PASJ, 59, S113

Jansen, F., et al. 2001, A&A, 365, L1

Kalberla, M., et al. 2005, A&A, 440, 775

Kargaltsev, O., & Pavlov, G. G. 2008, in AIP Conf. Proc., 983, 40 Years of Pulsars: Millisecond Pulsars, Magnetars and More, ed. Bassa et al. (New York: AIP), 171

Kokubun, M., et al. 2007, PASJ, 59, S53

Koyama, K., et al. 2007, PASJ, 59, S23

Kushino, A., Ishisaki, Y., Morita, U., Yamasaki, N. Y., Ishida, M., Ohashi, T., & Ueda, Y. 2002, PASJ, 54, 327

Table 1. Journal of the observations

	Obs ID	Observation date	Aim point[*]	Effective Exposure (ks)
Suzaku	504034010	2010/01/13–2010/01/16	$(314°409, -0°145)$	104
XMM-Newton	0504990101	2007/08/09	$(314°362, -0°143)$	$21/22/15^{\dagger}$

[*] In Galactic coordinates.

[†] The effective exposures for MOS1/MOS2/pn.

Manchester, R.N., et al. 2005, AJ, 129, 1993

Mattana, F., et al. 2010, ApJ, 694, 12

Mitsuda, K., et al. 2007, PASJ, 59, S1

Nakamura, R., et al. 2009, PASJ, 61, S197

Nakamura, R., Bamba, A., Dotani, T., Ishida, M., Yamazaki, R., & Kohri, K. 2012, ApJ, 746, 134

Nolan, P. L., et al. 2012, ApJS, 199, 31

Prigozhin, G., Burke, B., Bautz, M., Kissel, S., Lamarr, B. 2008, IEEE Transactions on Electron Devices, 55, 2111

Serlemitsos, P., et al. 2007, PASJ, 59, S9

Strüder, L., et al. 2001, A&A, 365, L18

Takahashi, T., et al. 2007, PASJ, 59, S35

Turner et al. 2001, A&A, 365, L27

Tawa, N., et al. 2008, PASJ, 60, S11

Uchiyama, H., et al. 2009a, PASJ, 61, S9

Uchiyama, H., et al. 2009b, PASJ, 61, S189

Yamauchi, C., et al. 2011, PASP, 123, 852

Yamazaki, R., Kohri, K., Bamba, A., Yoshida, T., Tsuribe, T., & Takahara, F. 2006, MNRAS, 371, 1975
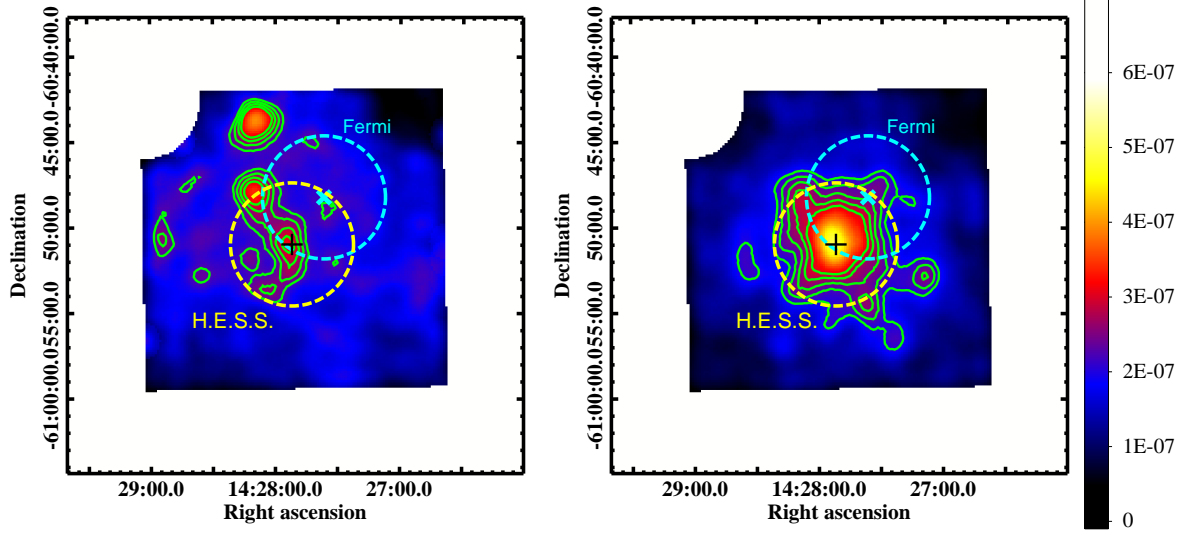
Fig. 1. XIS images of the HESS J1427–608 field in the 0.5–2 keV (left) and the 2–8 keV (right) bands, respectively. The color bar indicates the surface brightness in units of count s^{-1} $pixel^{-1}$. The black cross and the dashed yellow circle indicate the position and the extent of the VHE source (3′.6 in radius)[1], respectively. The cyan cross and the dashed cyan circle indicate the position and the error circle of 2FGL J1427.6–6048c (3′.6 in radius), respectively (Nolan et al. 2012). The green contours indicate the intensity of XIS image in linear scale.

Fig. 2. The source and the off-source regions are indicated in the XIS hard band image. The contours shown in figure 1 are also overlaid. The source region is defined within the circle of $r = 4′.5$ drawn by the solid line. The off-source region is defined as an annulus with an inner and an outer radius of $r = 6′.5$ and $r = 7′.5$ respectively, drawn by the dashed lines.

11

Table 2. The best-fit parameters of the observed XIS spectrum in the annulus region

	Soft	Medium	High
$N_{\rm H}$ (10^{22} cm^{-2})	$0.21^{+0.17}_{-0.16}$	$1.04^{+0.25}_{-0.19}$	$4.95^{+10.86}_{-1.49}$
kT (keV)	0.26 ± 0.06	$0.55^{+0.11}_{-0.08}$	$3.71^{+11.45}_{-1.53}$
Absorbed flux*	$0.86^{+1.58}_{-0.66}$	3.30 ± 1.06	$3.80^{+4.94}_{-1.90}$
	Abundance ($z_\odot$)		
Ne	0.57 (fixed)		
S	1.27 (fixed)		
Ar	2.10 (fixed)		
others	0.33 (fixed)		
Line E (keV)	$6.47^{+0.22}_{-0.07}$		
Line flux†	$7.0^{+3.9}_{-3.5}$		
χ^2/d.o.f	84.68 / 60		

* In units of 10^{-12} erg s^{-1} cm^{-2} in the 0.8–10 keV band.

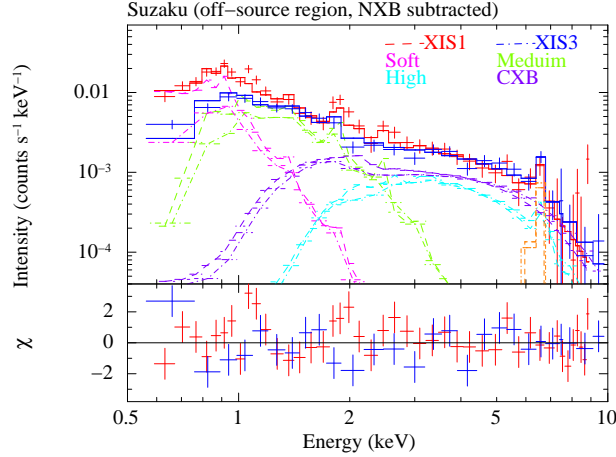† In units of 10^{-5} photons s^{-1} cm^{-2}.

Fig. 3. XIS spectra of the off-source region after NXB subtraction. Red and blue data represent XIS1 and XIS3 spectra, respectively. The best-fit model of thin thermal three temperature plasma with an iron emission line plus the CXB is also shown.
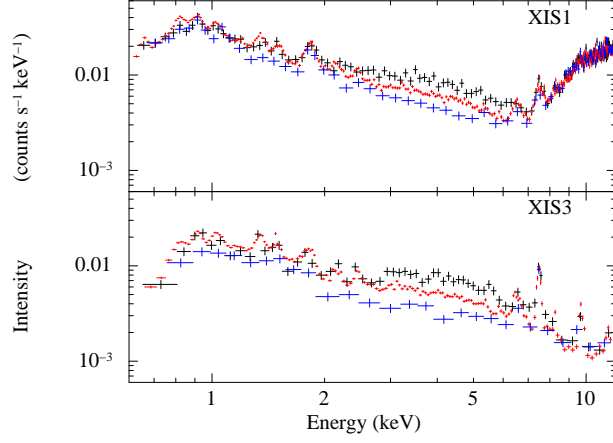
Fig. 4. Comparison of the source spectrum (black) including the background, the background spectrum estimated for the source region (red), and the off-source spectrum (blue). The off-source spectrum is normalized considering the area difference of source and off-source regions. The upper and lower panels show spectra of XIS1 and XIS3, respectively.
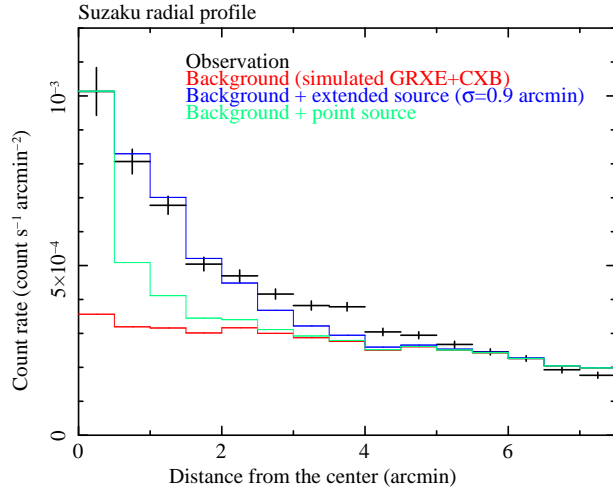

Fig. 5. The NXB subtracted, GRXE and CXB included radial profiles of XIS in the 2–8 keV band. Black, red, blue and green lines represent the observed radial profile, the simulated radial profile of GRXE+CXB, that of an extended source with $\sigma = 0\rlap{.}'9$ and GRXE+CXB, and that of a point source and GRXE+CXB, respectively.
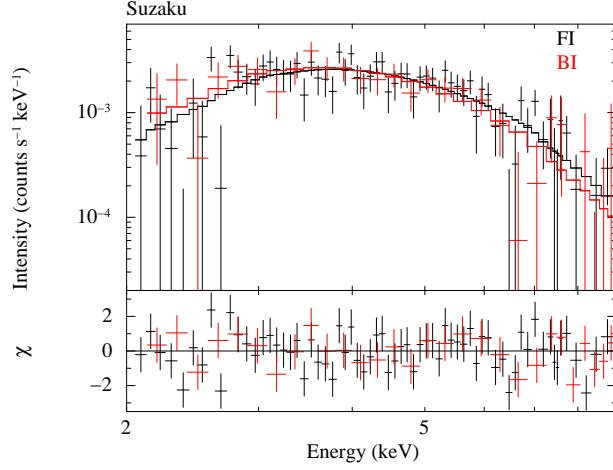
13

Fig. 6. The background-subtracted energy spectra of Suzaku J1427–6051. Black and red crosses indicate data of FI CCDs (sum of XIS0 and XIS3) and BI CCD (XIS1), respectively. The solid lines show the best-fit absorbed power-law model.

Table 3. The best-fit parameters of the XIS spectrum

	Power-law	APEC
N_{H} (10^{22} cm^{-2})	$11.1^{+2.9}_{-2.5}$	$9.0^{+2.2}_{-1.9}$
Γ	$3.1^{+0.6}_{-0.5}$	—
kT (keV)	—	$3.2^{+1.5}_{-0.8}$
Abundance ($z_\odot$)	—	< 0.09
Unabsorbed flux*	$8.9^{+3.6}_{-2.0}$	$6.6^{+4.7}_{-2.5}$
Absorbed flux*	3.1	3.0
χ^2/d.o.f.	64.02/71	62.89/70

Note: The errors are in the 90 % confidence range.

* In the 2.0–10.0 keV band in units of 10^{-13} erg s^{-1} cm^{-2}.

Table 4. Point sources detected with XMM-Newton

ID	Name	Distance[*]	MOS Count rate[†]	
			0.3–2 keV	2–12 keV
X1	XMMU J142755.4–605112.9	$0\!\!.\!\!'47$	5.3	3.3
X2	XMMU J142746.5–605011.4	$1\!\!.\!\!'05$	—	1.9
X3	XMMU J142746.8–605317.8	$2\!\!.\!\!'27$	2.3	—
X4	XMMU J142800.7–605356.4	$3\!\!.\!\!'13$	2.7	—
X5	XMMU J142731.4–605141.4	$2\!\!.\!\!'59$	—	2.9
X6	XMMU J142810.3–604752.0	$3\!\!.\!\!'85$	3.3	1.7
X7	XMMU J142736.9–604712.8	$4\!\!.\!\!'21$	1.9	—
X8	XMMU J142711.0–605320.3	$5\!\!.\!\!'51$	—	2.2
X9	XMMU J142742.7–604436.9	$6\!\!.\!\!'48$	3.4	—
X10	XMMU J142722.3–604425.8	$7\!\!.\!\!'50$	—	3.1
X11	XMMU J142856.1–605027.9	$7\!\!.\!\!'83$	3.0	—
X12	XMMU J142649.9–604810.0	$8\!\!.\!\!'08$	—	1.7
X13	XMMU J142810.0–604337.9	$7\!\!.\!\!'69$	9.1	—
X14	XMMU J142651.3–605300.9	$7\!\!.\!\!'65$	4.9	—
X15	XMMU J142654.9–604556.1	$8\!\!.\!\!'60$	4.1	—
X16	XMMU J142855.6–604636.4	$8\!\!.\!\!'92$	3.1	—

[*] Angular distance from the center of Suzaku J1427–6051.

[†] Sum of MOS1 and MOS2 count rate in units of 10^{-3} count s^{-1}.
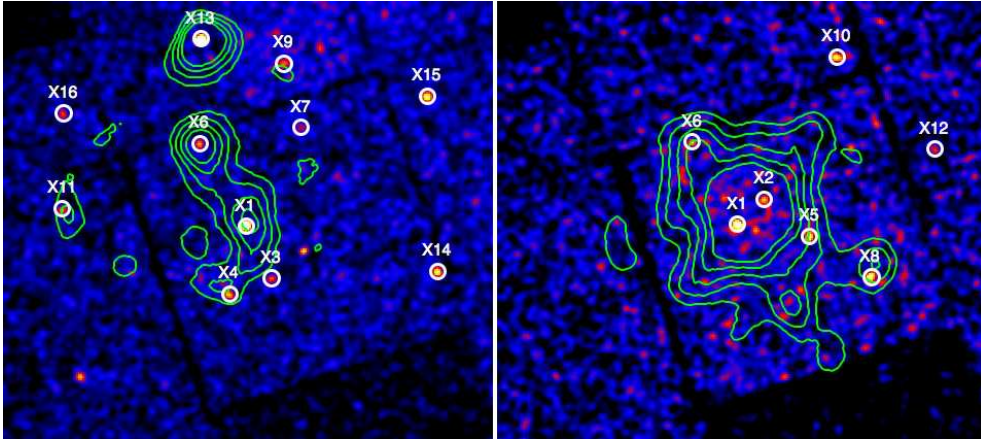

Fig. 7. The summed MOS images of the HESS J1427–608 field in the 0.3–2 keV band (left) and in the 2–12 keV band (right), respectively. The green contours indicate the XIS images shown in figure 1. The white circles indicate the point sources detected by the SAS tool `edetect_chain`, which are listed in table 4.
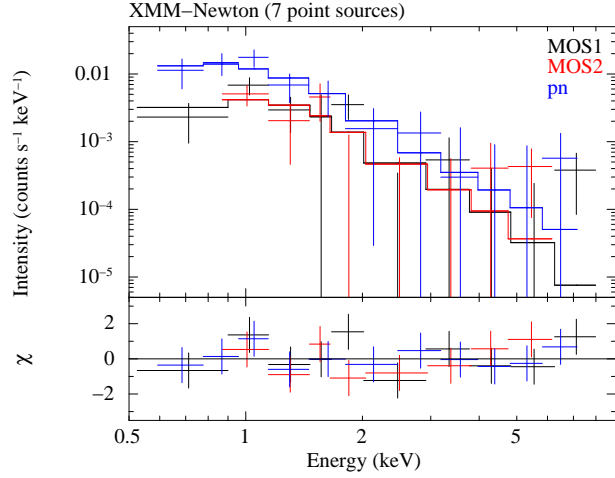
Fig. 8. The summed spectrum of seven point sources detected with XMM-Newton. Black, red and blue crosses indicate MOS1, MOS2 and pn spectra, respectively. The solid lines show the best-fit absorbed power-law model.

Table 5. The best-fit parameters of EPIC spectra

	X1	Sum of X1–X7
N_H (10^{22} cm^{-2})	< 0.3	0.3 ± 0.1
Γ	3.1 (fixed)	3.1 (fixed)
Unabsorbed flux*	$0.7^{+0.4}_{-0.2}$	$1.7^{+0.7}_{-0.6}$
Absorbed flux*	0.7	1.7
χ^2/d.o.f.	11.28 / 6	16.74 / 27

Note: The errors are in the 90 % confidence range.

*In the 2–10 keV band in units of 10^{-14} erg s^{-1} cm^{-2}.
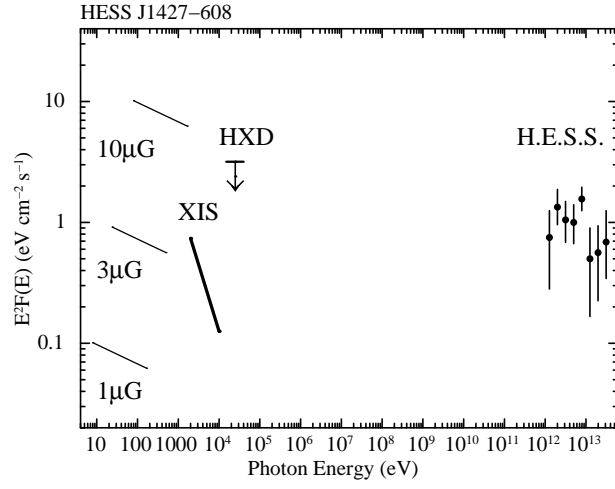
16

Fig. 9. Spectral energy distribution of HESS J1427–608 from X-ray through VHE gamma-ray is shown. The calculated spectra of the synchrotron emission are overlaid. The H.E.S.S. spectrum is taken from Aharonian et al. (2008).